

# Effect of Plastic Hot Deformation on the Hardness and Continuous Cooling Transformations of 22MnB5 Microalloyed Boron Steel

A. BARCELLONA and D. PALMERI

The strains, transformation temperatures, microstructure, and microhardness of a microalloyed boron and aluminum precoated steel, which has been isothermally deformed under uniaxial tensile tests, have been investigated at temperatures between 873 and 1223 K, using a fixed strain rate value of  $0.08 \text{ s}^{-1}$ . The effect of each factor, such as temperature and strain value, has been later valued considering the shift generated on the continuous cooling transformation (CCT) diagram. The experimental results consist of the starting temperatures that occur for each transformation, the microhardness values, and the obtained microstructure at the end of each thermomechanical treatment. All the thermomechanical treatments were performed using the thermomechanical simulator Gleeble 1500. The results showed that increasing hot prestrain (HPS) values generate, at the same cooling rate, lower hardness values; this means that the increasing of HPS generates a shift of the CCT diagram toward a lower starting time for each transformation. Therefore, high values of hot deformations during the hot stamping process require a strict control of the cooling process in order to ensure cooling rate values that allow maintaining good mechanical component characteristics. This phenomenon is amplified when the prestrain occurs at lower temperatures, and thus, it is very sensitive to the temperature level.

DOI: 10.1007/s11661-009-9790-8

© The Minerals, Metals & Materials Society and ASM International 2009

## I. INTRODUCTION

INCREASING strength requirements for structural steel components in vehicles, aiming to reduce the weight of cars while preserving their safety characteristics, have brought increasing use of hot forming operations. The method of press quenching, using manganese boron steels, allows steels to achieve strengths greater than 1500 MPa. In these steels, high formability and high mechanical strength can be achieved in two different production process steps of a finished part. The required strengths in the components can be obtained by heating at least to the austenitizing temperature, where the material has an fcc structure, and then cooling sufficiently quickly. An aluminum-silicon surface coating protects against oxidation of the base material. The cooling rate during the hot forming operations is strongly dependent on the surface press level; therefore, there are different cooling conditions in the various areas of a press-quenched component.

The physical properties and the performance of these components are greatly influenced by the microstructure, residual stresses, and geometrical defects imposed by the manufacturing process. In order to efficiently develop these products, it is necessary to quickly

simulate and analyze the manufacturing processes to predict the final microstructure. Proper simulation tools are computational numerical models or neuro-fuzzy models and require accurate material data. Unfortunately, for this innovative material, the continuous cooling transformations (CCTs) have been determined only on the thermally treated material, but little knowledge exists on the CCTs that reproduce the typical work conditions of the press quenching process. The purpose of this work is to describe the employed experimental methods to obtain the hardness and microstructural changes of prestrained and thermally treated microalloyed boron steel 22MnB5.<sup>[1-3]</sup>

## II. 22MnB5 ALUMINUM PRECOATED STEEL PROPERTIES

Quenchable boron steels use this alloying element as a hardening agent during thermomechanical treatments and provide a material with excellent hardness and high strength. The quenching treatment, usually performed on these materials, determines the heterogeneous precipitation of boron carbide at the grain boundaries and also the boron segregation. The segregation phenomenon causes increasing hardenability of the material by suppressing the austenite to ferrite transformation.<sup>[4-6]</sup> Substitutional solid solution elements such as Mn are known to only slightly influence the strength after quenching; however, Mn is essential for securing hardenability.

Hot stamping is a nonisothermal forming process for sheet metals, where forming and quenching take place in

---

A. BARCELLONA, Associate Professor, and D. PALMERI, Assistant Researcher, are with the Dipartimento di Tecnologia Meccanica, Produzione ed Ingegneria Gestionale, University of Palermo, Viale delle Scienze, 90128 Palermo, Italy. Contact e-mail: palmeri@dtm.unipa.it

Manuscript submitted July 18, 2008.

Article published online February 26, 2009

one combined process step. During the forming process, the material, which is in the austenitic phase, has good formability coupled with low mechanical strength. After the deformation step, the material is quenched directly inside the stamping, attaining high mechanical strength at the end of the deformation process. The thermomechanical cycle carried out during the working process allows manufacturers to obtain final products with complex shape and high mechanical strength. Before hot stamping, the microstructure of these materials is the ferritic-pearlitic type; after the stamping step, the microstructure may achieve a totally martensitic morphology.

The best cooling rate for quenching is determined by the conditions that avoid transforming the austenite into ferrite, pearlite, and bainite transformations, and the rates also depend on the chemical composition of steel. The prior austenite grain size plays a key role in beginning the diffusion transformations. When the austenite grain size becomes smaller, or the heating temperature becomes lower, the transformations into these phases take place quicker and, as a consequence, the cooling rate for the quenching must be higher.

Based on these considerations, the effect of the hot prestrain (HPS) level on the beginning of the austenite phase transformation has been determined. The hot stamping process requires that the sheet be brought to a temperature of 1223 K, put inside the dies, and then deformed and simultaneously quenched. Before the hot stamping process, these steels exhibit respective yield stress and ultimate tensile strength values of 400 and 600 MPa. The maximum elongation percentage value is equal to 21 pct. After the hot deformation and quenching process, the yield and the ultimate tensile strengths increase to respective values of 1000 and 1500 MPa. The maximum elongation until fracture decreases to 5 pct.

In order to avoid surface oxidation and decarburization phenomena during the hot stamping operations, the sheets are usually covered with a layer of Al-Si. Through the hot forming process, the coated surface changes from Al-10 pct Si to Fe-Al(Si) phase. The melting temperature of Al-10 pct Si is equal to 873 K, but during the heating, the Fe-Al alloy layer, with high melting point, is formed. The presence of the Fe-Al(Si) surface layer also determines a good paintability without phosphating treatments. Therefore, the 22MnB5 coated steel simultaneously has good formability and improved corrosion resistance. Usually, the thickness of the coating layer is equal to 20 to 30  $\mu\text{m}$ .

The hot material is stamped inside cold dies and the deformation process is coupled with the quenching process. The achieved microstructure, in the best conditions, is composed of martensite; thus, the control and prediction of microstructural growth and the related mechanical properties of steels are fundamental for steel manufacturers. In order to achieve this purpose, the measurement and the prediction of transformation kinetics are strongly needed. The most important information that can be provided from a nonisothermal analysis is start and finish transformation temperatures and kinds and volume fractions of transformed products. Such characteristics of thermal transformations are usually studied with CCT curves, in which the start and

end transformation temperatures are displayed for different cooling paths. Based on the CCT diagrams, the suitable cooling parameters for producing steels with desired microstructure can be determined.<sup>[6-12]</sup>

### III. CCT AND CCT HPS DIAGRAMS

By means of the hot deformation simulator Gleeble 1500 (Arcelor, University of Erlangen-Nuremberg, Bavaria, Germany), hot tensile tests were performed on standardized tensile test specimens laser cut from sheets 1.75-mm thick. These experiments allowed determination of the complete CCT diagrams for the 22MnB5 steel under prestrain conditions. The Gleeble 1500 thermomechanical simulator is able to heat the specimens by direct resistance heating. A low voltage current passes directly through the specimen and the resistance of the specimen itself generates Joule heating. Currents of several thousand amperes can be supplied to enable very fast heating rates. Temperature measurements were performed with thin wire thermocouples, of Ni/Cr-Ni type, welded to the surface of the specimen, as shown in Figure 1. A closed loop feedback signal enables precise control of the heat input based on the temperature at any instant.

The specimens were austenitized for 4 minutes in order to obtain a homogeneous austenitic microstructure before the thermomechanical treatment. Each set of experiments had differing temperature in which the mechanical treatment was performed and differing prestrain value. Each group of experiments includes eight different cooling rates arising from increasing air pressure during cooling. The cooling rate depends on the air pressure value and even on the temperature at which the cooling starts. The cooling rates were evaluated both in the case without prestrain, when the cooling starts directly from the austenitizing temperature, and in the case in which the HPS is performed at different temperatures.

For each group of experiments, a small difference in the cooling rate range was observed. Furthermore, the necessity to bring the material to different deformation temperatures produces different values of delay in the start of the deformation process. This delay may generate a noise in the search of the prestrain level influence on the transformation temperature, and thus special attention was paid to evaluate this phenomenon. This value of delay becomes higher when the deformation temperature is equal to 873 K, and in this case, the final microstructure observations depend both on the movement of the transformation temperature and on the delay in the start of transformations (Figure 2).

Three temperature values were selected for executing of the mechanical treatment 1073, 973, and 873 K. This choice was suggested by considering the bainite start ( $B_S$ ) temperature for isothermal transformation equal to 831 K depending on the chemical composition of steel, as shown in Eq. [1].<sup>[13,14]</sup>

$$B_S(^{\circ}\text{C}) = 830 - 270 \text{ wt pct C} - 90 \text{ wt pct Mn} \\ - 37 \text{ wt pct Ni} - 70 \text{ wt pct Cr} - 83 \text{ wt pct Mo} \quad [1]$$

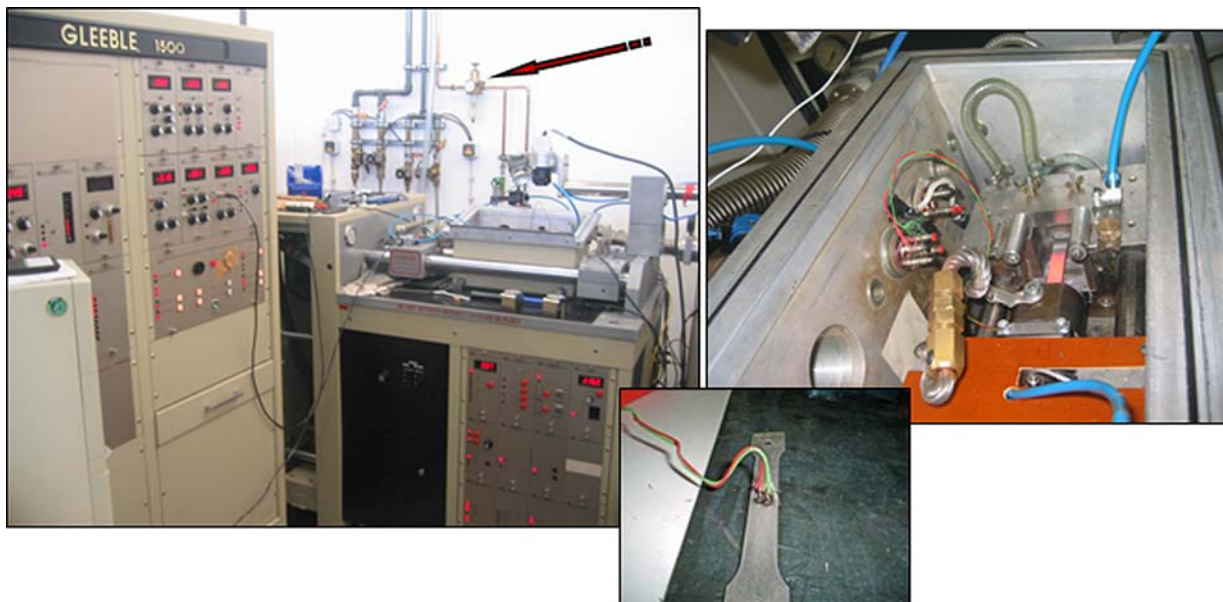


Fig. 1—Thermomechanical simulator Gleeble 1500.

Therefore, the mechanical treatment temperatures were selected inside the range  $A_3$  to  $B_S$ , where  $A_3$  is the equilibrium temperature between the austenite and ferrite phases. The entire experimental scheme is highlighted in Table I.

After each set of experiments, the cooling curves were recorded for each cooling rate. In order to amplify the difference in the slope of the cooling curves, numerical computation of the gradient of each cooling curve was performed. The gradient curves make it easier to highlight the transformation temperatures, because the curves are very sensitive to slope change. The typical chemical composition of hot stamping boron steels is 0.2 to 0.4 pct C, 1.1 to 1.3 pct Mn, 1.5 to 3.5 pct Si, 1.5 to 3 pct Cr, and finally the boron B with percentage 0.002 to 0.004 pct. The boron enables the ferritic zone to shift toward the lower cooling rate and thus ensures a good quenchability during the heat treatments.

The attained prestrain value was determined using the optical deformation measurement system ARAMIS. This system provides the local deformations for a defined surface. The ARAMIS system is positioned in front of a tensile test specimen; a stochastic pattern is applied on the surface of each specimen using a hot resistant color spray (boron nitride spray), following guidelines that guarantee a regular and reproducible pattern on the specimen. The complete deformation behavior of the specimen can be captured and evaluated during the deformation process by recording and evaluating numerous images. In this research, the prestrain level was selected varying the displacement of the specimen clamping device and was measured with the ARAMIS system. The performed analysis determined the influence of the HPS level on the CCT curve shapes (Figures 3 through 6).

#### IV. MICROSTRUCTURE AND MICROHARDNESS RESULTS

After the thermomechanical treatments, microhardness Vickers tests (test load 1000 grams) and micrographic observations by light optical metallographic analysis were performed. The middle cross section of each specimen was prepared for micrographic observation using standard techniques by grinding with SiC abrasive followed by polishing on velvet cloth using diamond paste with 1- $\mu\text{m}$  mean grain dimension. All the samples were chemically etched using 2 pct Nitric acid for times dependent on the thermomechanical cycle.

During the deformation process, there are two different phenomena that influence the final properties of material: the increasing the dislocation density and the decreasing mean free paths of dislocations. Therefore, a strong influence can be produced from the prestrain level on the final microstructural properties, depending on the occurred recrystallization phenomena. The obtained microhardness values were even related to the micrographic observation in order to highlight the kind of phenomena that influence the mechanical properties of the material.

The micrographic observations for each set of experiment have been performed considering three different magnification values, in order to make possible the analysis of recrystallization phenomena and of different phases. Only at higher magnification, such as 1250 times, is it possible to distinguish the surface relief associated with the granular bainite phase transformation; therefore, it is possible to highlight the kind of transformation that occurs, either diffusive or diffusionless. At low magnification, it is possible to see mixed microstructures with different dimensions vs the one produced from the recrystallization phenomenon of austenite grains. The microstructural observations showed that low prestrain

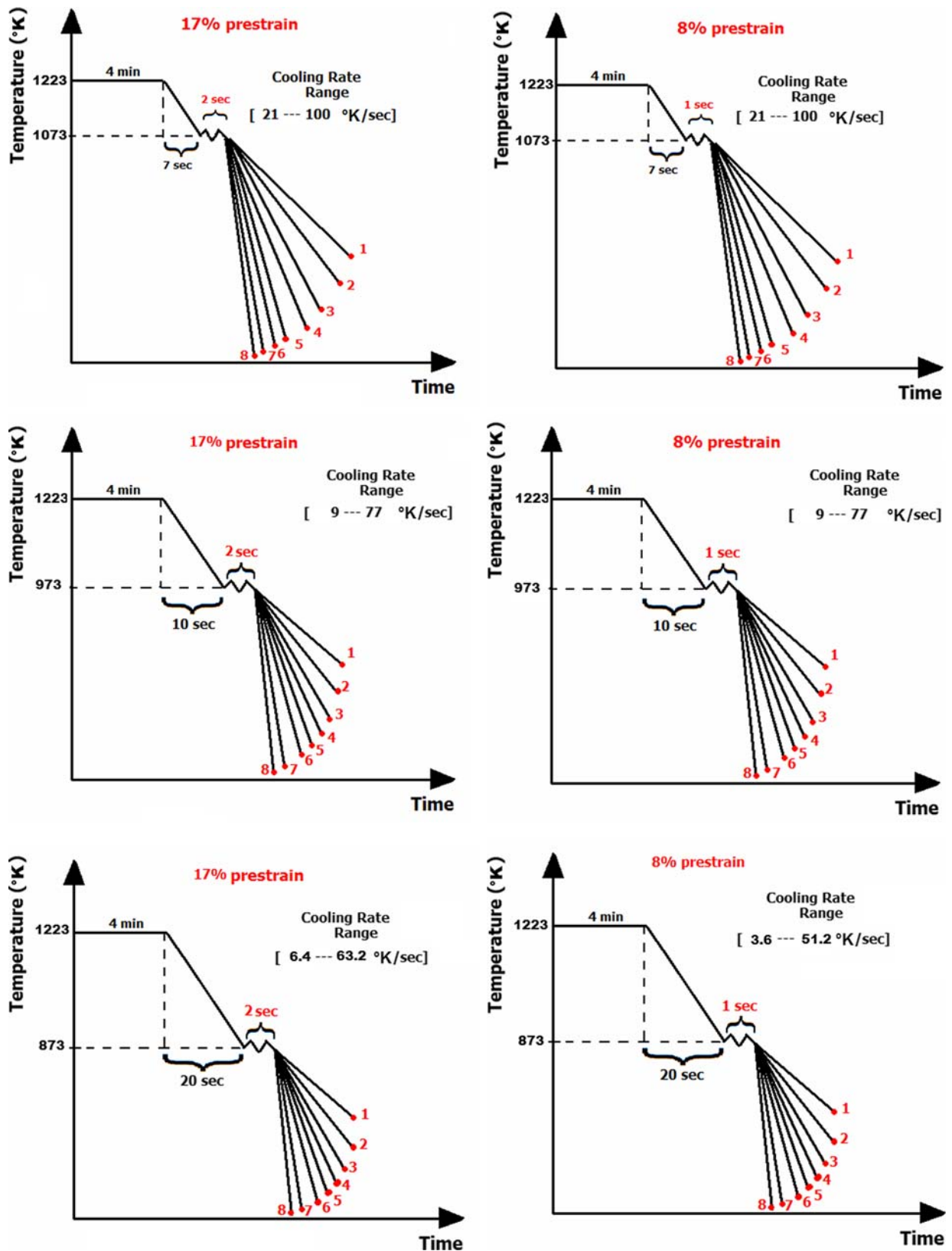


Fig. 2—Experimental condition: cooling rate ranges and cooling start delays.

values increase the mean grain dimension as well as decreasing amounts of ferrite. Low values of prestrain promote diffusionless transformation of the austenitic

phase, and thus produce better mechanical properties. Higher values of prestrain cause stresses that exceed the maximum flow stress; therefore, the final material

properties are slightly affected by the amount of ferritic phase amount (Figures 7 through 13(b)). Starting from the micrographic results, and coupling them with the thermomechanical analysis previously mentioned, the CCT curves were produced.<sup>[15-21]</sup>

**Table I. Experimental Scheme: Thermal and Thermomechanical Treatments**

Temperature (K)	Prestrain (Pct)	Cooling Rate (Air Pressure in $10^5$ Pa)							
1223	no	1	2	3	4	5	6	7	8
1073	8	1	2	3	4	5	6	7	8
1073	17	1	2	3	4	5	6	7	8
973	8	1	2	3	4	5	6	7	8
973	17	1	2	3	4	5	6	7	8
873	8	1	2	3	4	5	6	7	8
873	17	1	2	3	4	5	6	7	8

## V. EXPERIMENTAL RESULTS

After 4 minutes at 1223 K and without prestrain conditions, the primary austenite grain size (PAGS) varied between 20 and 45  $\mu\text{m}$ , and the mean grain dimension decreased when the cooling rate increased. As shown in Figure 7, the mean grain dimension of the PAGS, in the case of the 22.2 K/s cooling rate, is lower and varies between 10 and 32  $\mu\text{m}$ . The martensite starting point, when the martensitic transformation occurs, begins at 683 K and ends at 583 K. Cooling rates up to 35 K/s, and therefore when the cooling air pressure is higher than  $3 \times 10^5$  Pa, a fully martensitic microstructure is achieved. At lower cooling rate, bainite and even ferrite can be formed resulting in lower microhardness level, as shown in the Table II. The microhardness value of the martensite phase was 551 HV, whereas the presence of bainite led to a decreased hardness of 533 HV and the ferrite-pearlite microstructure had a lower hardness of 290 HV. During high-temperature isothermal mechanical treatment followed by continuous cooling, a particular kind of bainite transformation named granular bainite appears; it is a microstructure of ferrite matrix and islands of other phases. The island structure of granular bainite may be martensite and retained austenite; martensite, bainite, and retained austenite; or other metastable structures, which are a function of the composition of steel and the cooling rate. A single thermal cycle (deformation-free) was used as a reference for subsequent determinations of the hot deformation influence.

The first set of experiments with hot deformation conditions were performed at 1073 K considering two prestrain values equal to 8 and 17 pct. The coupled micrographic and microhardness study highlighted that, when the cooling rate is produced by an air pressure of 7 or  $8 \times 10^5$  Pa, for both the prestrain levels, the obtained microstructure is almost fully martensitic (Figures 8(b) and 9(b)). The granular bainitic transformation occurs at the lowering of cooling rate and produces lower microhardness values. The progressive softening of material with decreasing cool-

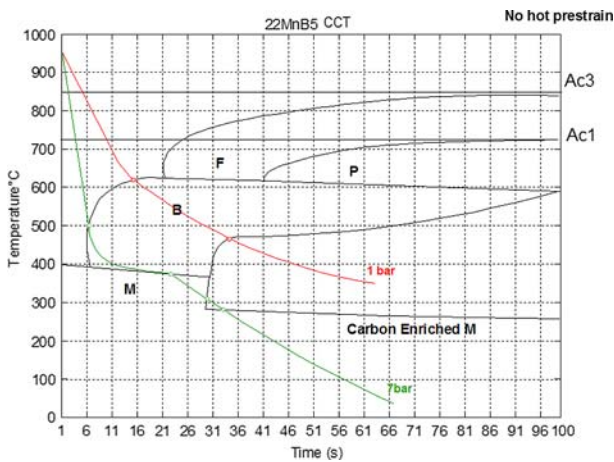


Fig. 3—CCT diagram without HPS.

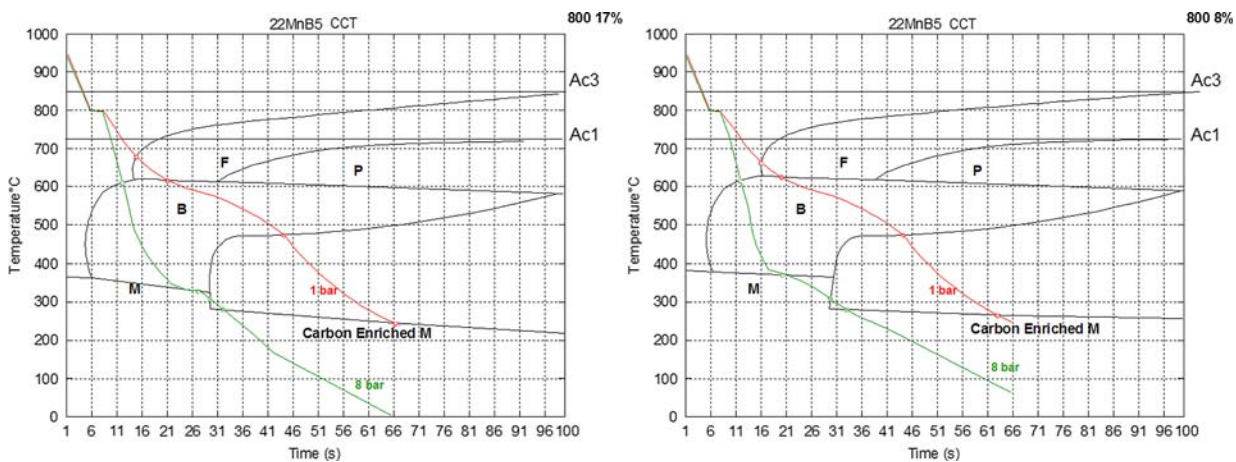


Fig. 4—CCT diagram 1073 K; HPS 17 and 8 pct.

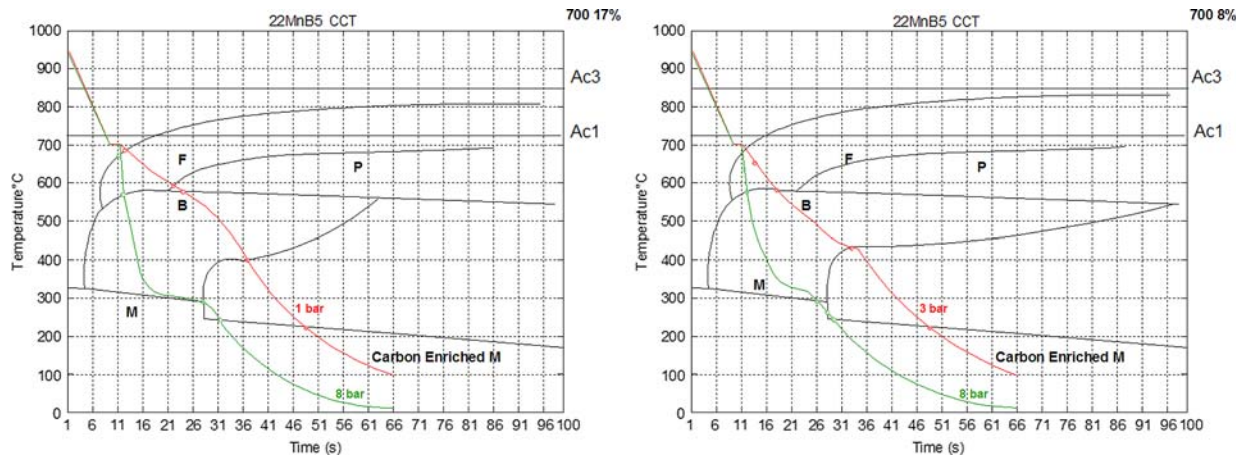


Fig. 5—CCT diagram 973 K; HPS 17 and 8 pct.

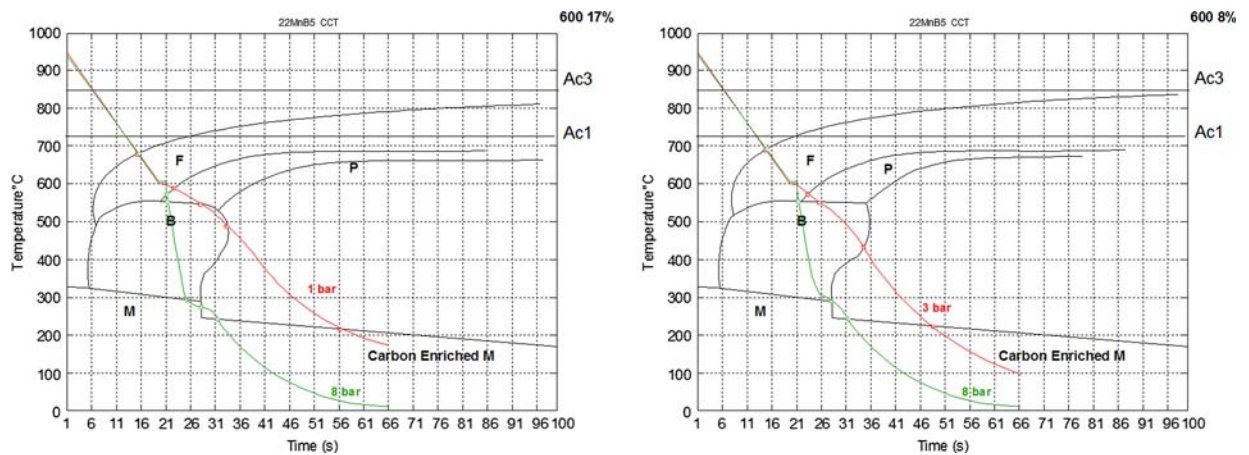


Fig. 6—CCT diagram 873 K; HPS 17 and 8 pct.

ing rate is much higher with the prestrain value of 17 pct and arises from the transformation of unstable austenite into ferritic-pearlitic and bainitic phases or a fully ferritic-pearlitic phase. The delay in the softening of material that is observed for lower HPS suggests that the CCT diagram is shifted toward the left side with increasing prestrain value. The thermomechanical simulation results allow determining the temperature range at which the martensitic transformation occurs; this range became smaller with increasing the hot deformation level. The  $M_s$  temperature attains a value of 653 K in the case of 8 pct of prestrain and a value of 643 K for 17 pct of prestrain. Also, the  $M_f$  temperature is shifted downward and attains respective values of 573 and 553 K for hot deformations of 8 and 17 pct. This lowering of the  $M_s$  and  $M_f$  temperatures with increasing prestrain value is also attributed to the shift of the CCT diagram.

The second set of experiments, considering the same HPS values (8 and 17 pct), was performed at 973 K in order to evaluate the effect of the hot deformation temperature on the material properties. The CCT diagrams exhibited  $M_s$  and  $M_f$  temperatures that ranged

between 613 and 563 K, and 573 and 533 K, respectively, for hot deformations of 8 and 17 pct.

The same values were found for the experiments executed at 873 K. The HPS generates a reduction of  $M_s$  and  $M_f$  temperatures, but this reduction becomes smaller when the temperature of HPS decreases. The microhardness results for the different operating conditions suggest that higher prestrain levels, even in this case, decrease the mechanical strength of the material. This phenomenon is influenced by the cooling rate and is higher when the cooling rate decreases. The softening phenomenon, already observed in the case of hot deformation temperature of 1073 K, is now amplified and starts earlier. In effect, as shown in Figures 10(a) through 11(b), only the cooling rate obtained with the  $8 \times 10^5$  Pa system allows attainment of an almost fully martensitic microstructure.

The highlighted material softening trends suggested that HPS produces a shift of the CCT diagram, and moreover an increase of prestrain value amplifies this occurrence. The observed shift of CCT diagram to the left side appears inhomogeneous with varying temperature. This phenomenon is amplified in the temperature

22MnB5\_1223°K

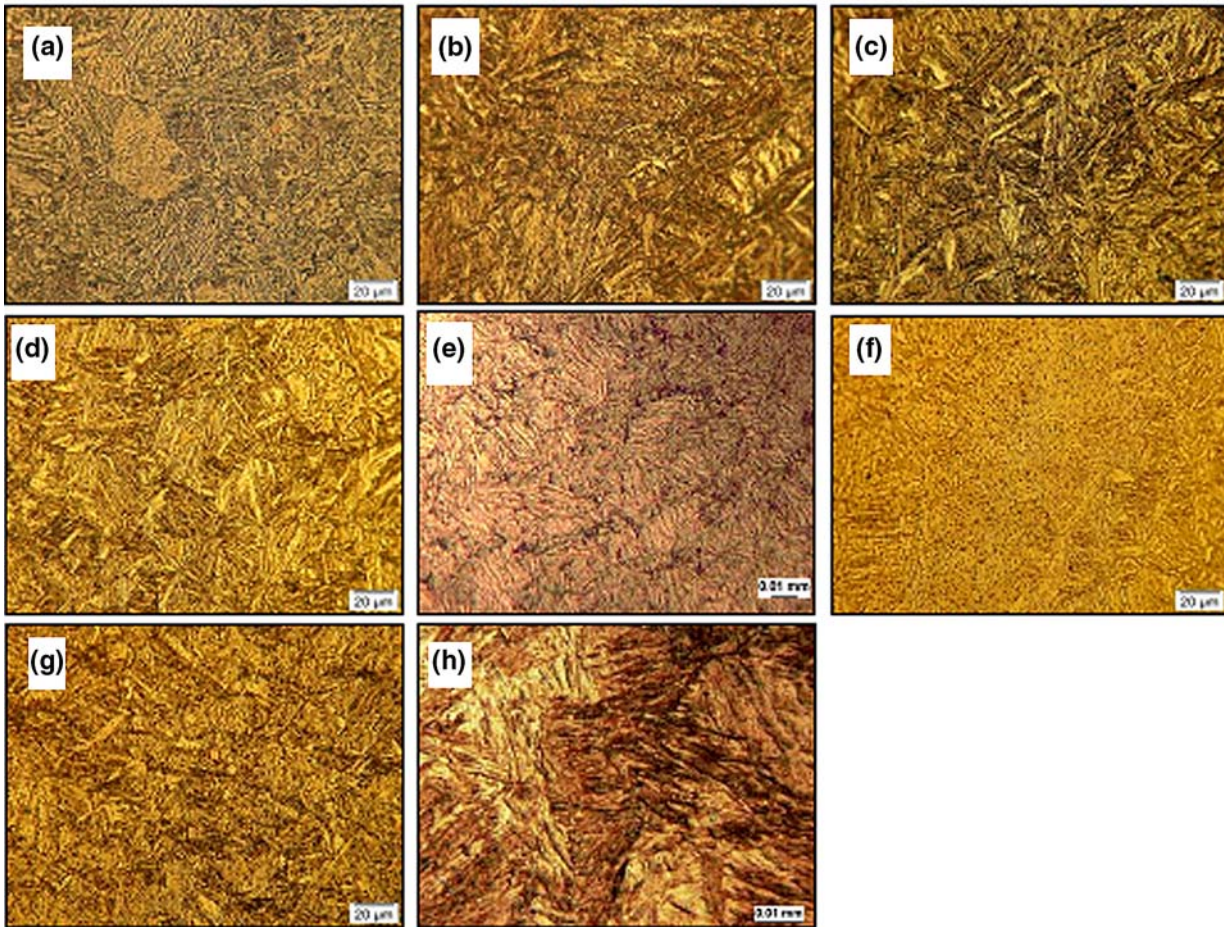


Fig. 7—Micrographic analysis without prestrain condition: (a)  $1 \times 10^5$  Pa cooling rate 22.1 K/s, (b)  $2 \times 10^5$  Pa cooling rate 32.1 K/s, (c)  $3 \times 10^5$  Pa cooling rate 48.8 K/s, (d)  $4 \times 10^5$  Pa cooling rate 56.6 K/s, (e)  $5 \times 10^5$  Pa cooling rate 62.9 K/s, (f)  $6 \times 10^5$  Pa cooling rate 68.3 K/s, (g)  $7 \times 10^5$  Pa cooling rate 73.1 K/s, and (h)  $8 \times 10^5$  Pa cooling rate 101.2 K/s.

range of diffusive pearlitic and ferritic transformations and became smaller in the field of bainitic transformations.

The obtained microstructures evidenced that the recrystallization process is now activated. In effect, the micrographic observations at low magnification (525 times) show a mixed microstructure with a PAGS ranging between values of 5 and 60  $\mu\text{m}$ . The occurrence of the PAGS refinement influences the kinetics of the austenitic diffusive transformations and thus the amount of ferrite and pearlite that can be formed during hot deformation. The austenitic grain size value causes dual and opposing effects on the material properties: a strengthening for grain refinement and a softening generated from the earlier starting of diffusive transformations as pearlite and ferrite when the grain size became smaller. For 8 pct hot deformations, the grain size refinement is activated even at a higher cooling rate, and thus, the microstructure contains a small amount of ferrite mixed with a martensitic-bainitic microstructure. This microstructure agrees with the obtained microhardness values.

At lower cooling rate, there is a progressive increase of ferrite and bainite phases. The decreasing of the HV

values is constant until the effect of the strengthening for grain refinement contrasts with the growing amount of the ferrite and pearlite. The same trends, but amplified, were found in the case of hot deformation temperature equal to 873 K.

It is necessary to state that, when the material is brought at 873 K before prestraining and quenching, actually, the deformed microstructure contains a small amount of diffusive phases; therefore, the recrystallization phenomenon of the austenite phase involves only a fraction of the material. This occurrence causes a recovery of microhardness at higher cooling rate, due to a smaller softening effect of grain refinement, although the material maintains the same microhardness trend observed in other cases. With decreasing temperature, it is possible to maintain a good microstructural result only with a low value of prestrain and a high value of cooling rate. In fact, only in this case does the effect produced from the recrystallization phenomenon as a strengthening factor predominate in the formation of ferritic regions that determine lower mechanical strength.

During hot forming operations, a strict control of the cooling process, especially for higher deformations, is

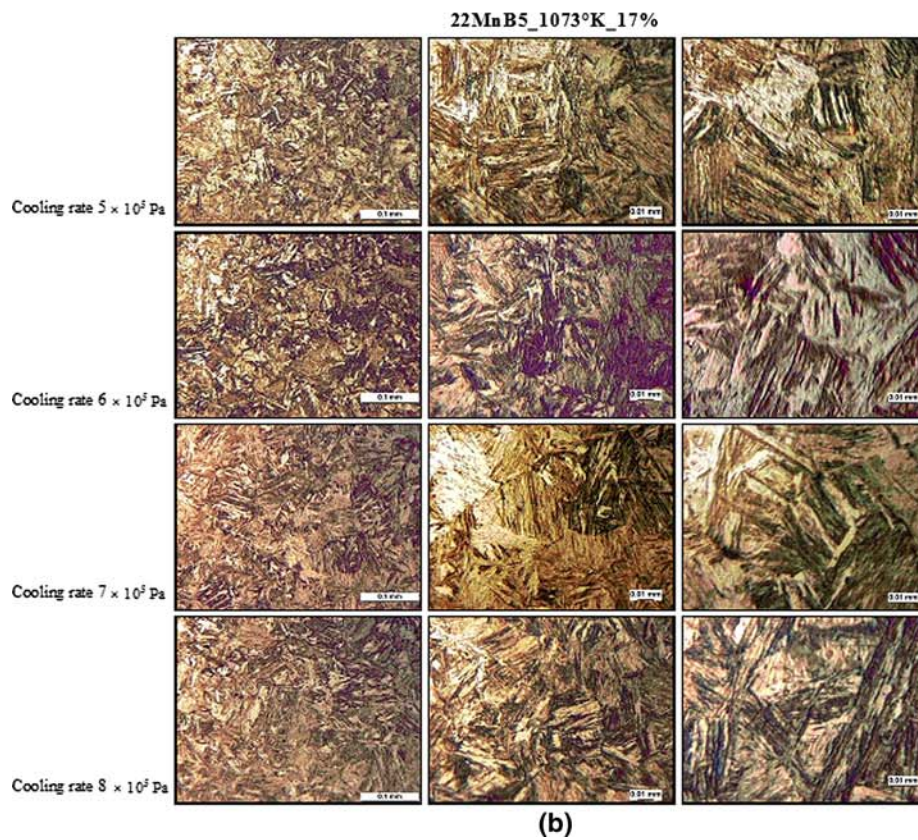
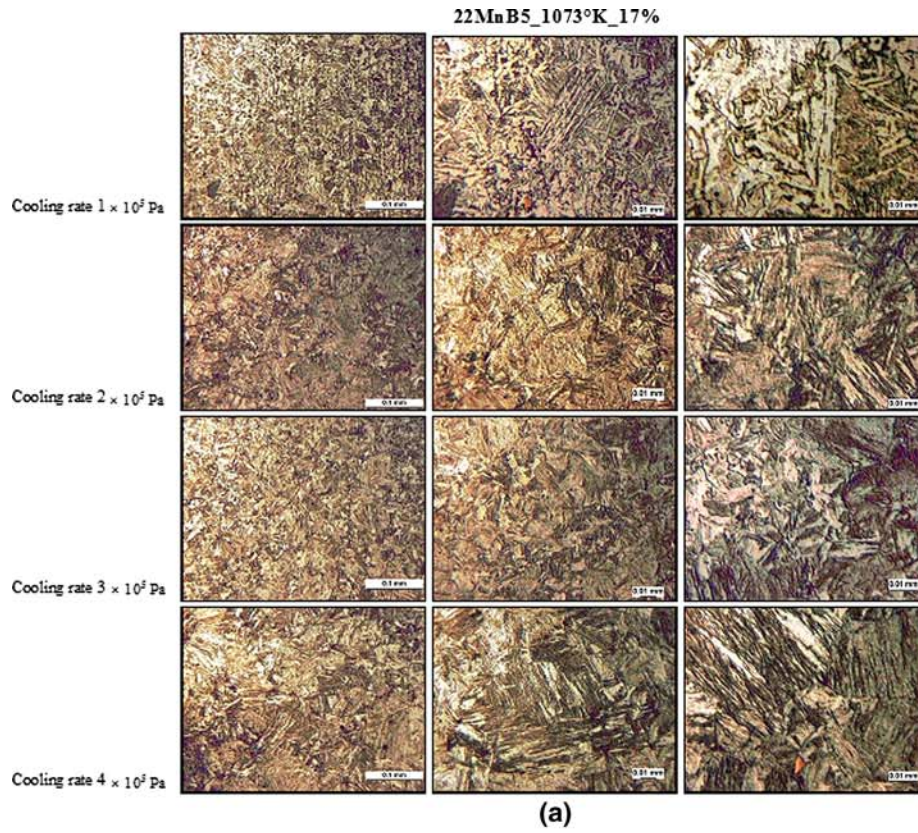


Fig. 8—(a) Micrographic analysis for four different cooling rates at 1073 K and 17 pct of prestrain (magnifications 250 times–525 times–1250 times);  $1 \times 10^5$  Pa cooling rate 21.1 K/s,  $2 \times 10^5$  Pa cooling rate 30 K/s,  $3 \times 10^5$  Pa cooling rate 45.2 K/s, and  $4 \times 10^5$  Pa cooling rate 52.3 K/s. (b) Micrographic analysis for four different cooling rates at 1073 K and 17 pct of prestrain (magnifications 250 times–525 times–1250 times);  $5 \times 10^5$  Pa cooling rate 58.6 K/s,  $6 \times 10^5$  Pa cooling rate 66.5 K/s,  $7 \times 10^5$  Pa cooling rate 72.1 K/s, and  $8 \times 10^5$  Pa cooling rate 100 K/s.



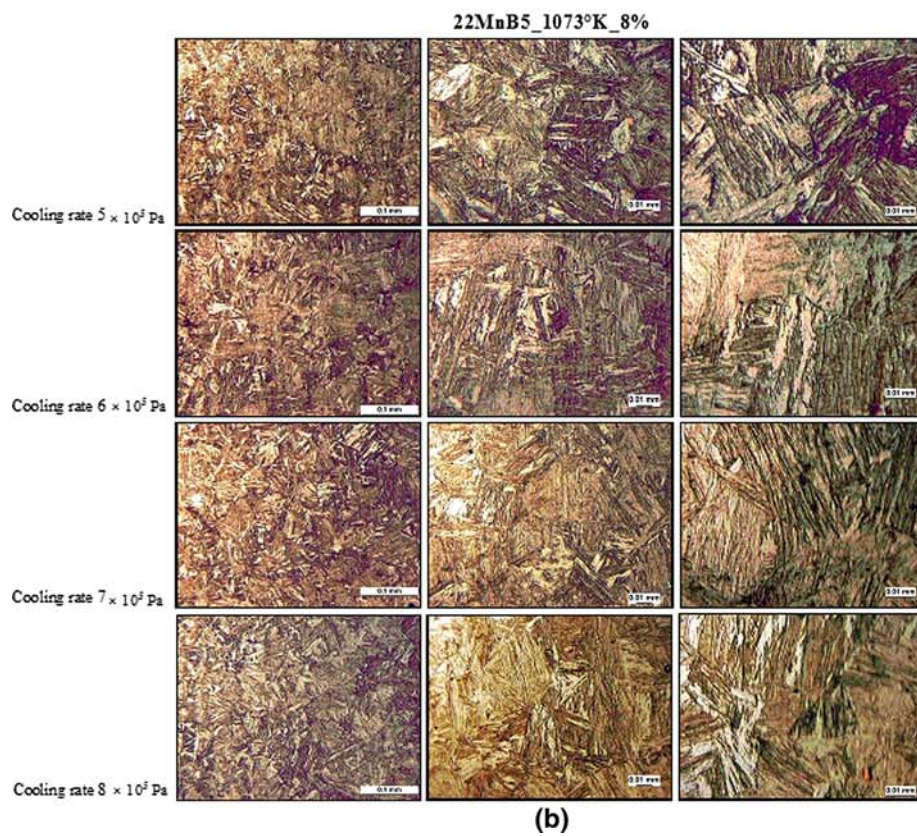
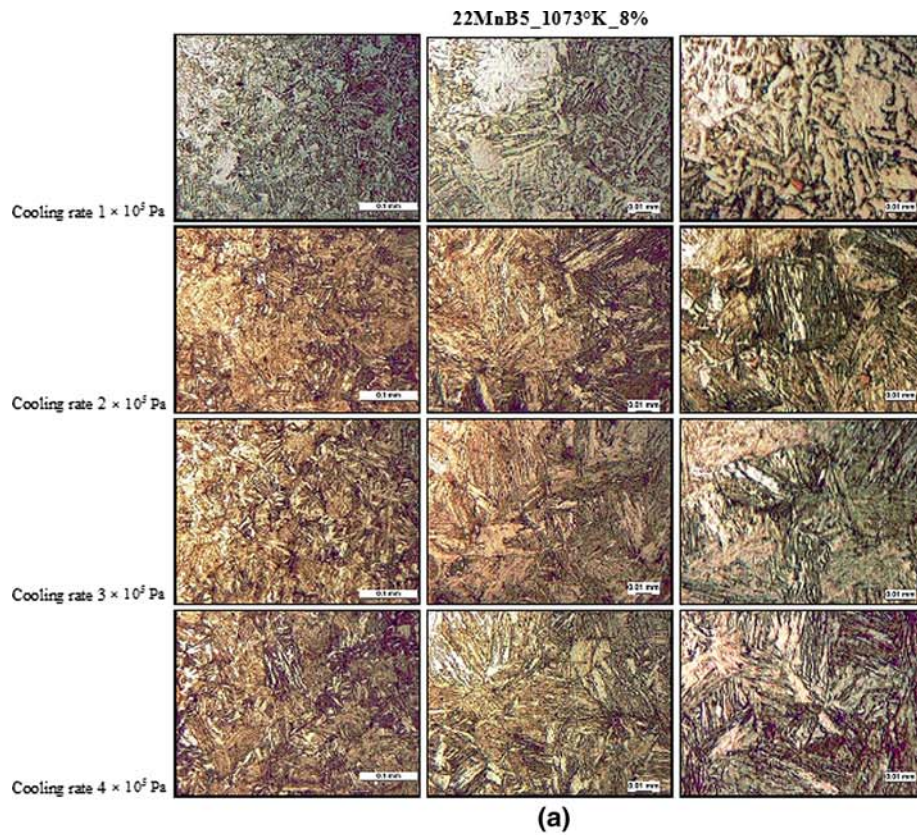


Fig. 9—(a) Micrographic analysis for four different cooling rates at 1073 K and 8 pct of prestrain (magnifications 250 times–525 times–1250 times);  $1 \times 10^5$  Pa cooling rate 21.1 K/s,  $2 \times 10^5$  Pa cooling rate 30 K/s,  $3 \times 10^5$  Pa cooling rate 45.2 K/s, and  $4 \times 10^5$  Pa cooling rate 52.3 K/s. (b) Micrographic analysis for four different cooling rates at 1073 K and 8 pct of prestrain (magnifications 250 times–525 times–1250 times);  $5 \times 10^5$  Pa cooling rate 58.6 K/s,  $6 \times 10^5$  Pa cooling rate 66.5 K/s,  $7 \times 10^5$  Pa cooling rate 72.1 K/s, and  $8 \times 10^5$  Pa cooling rate 100 K/s.

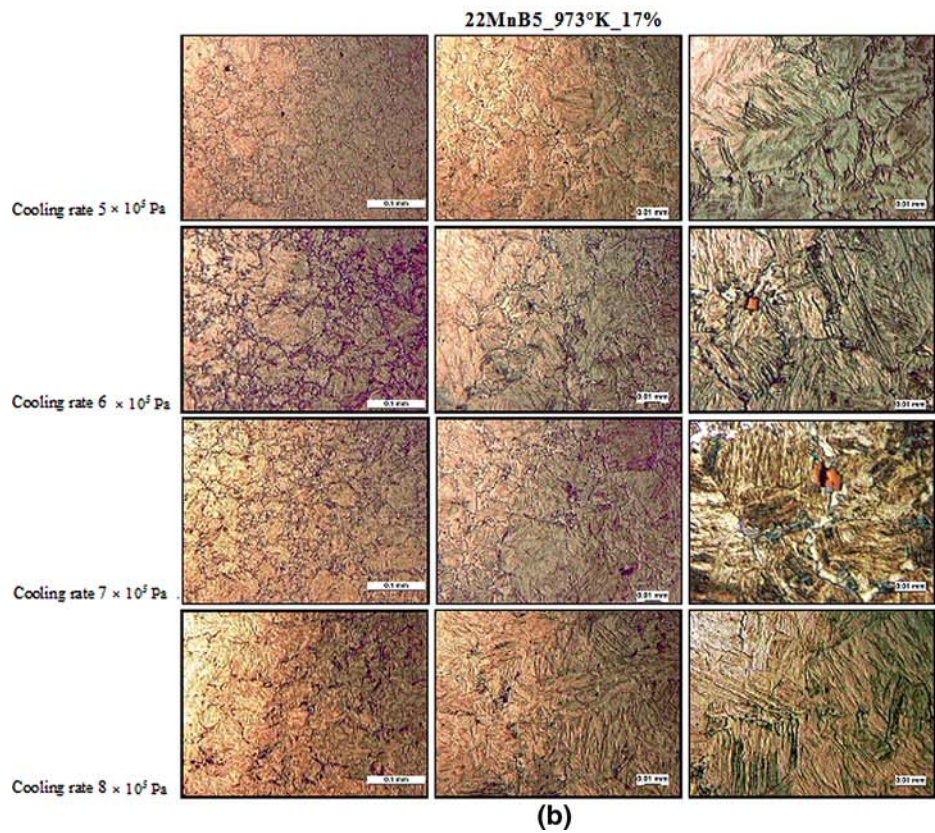
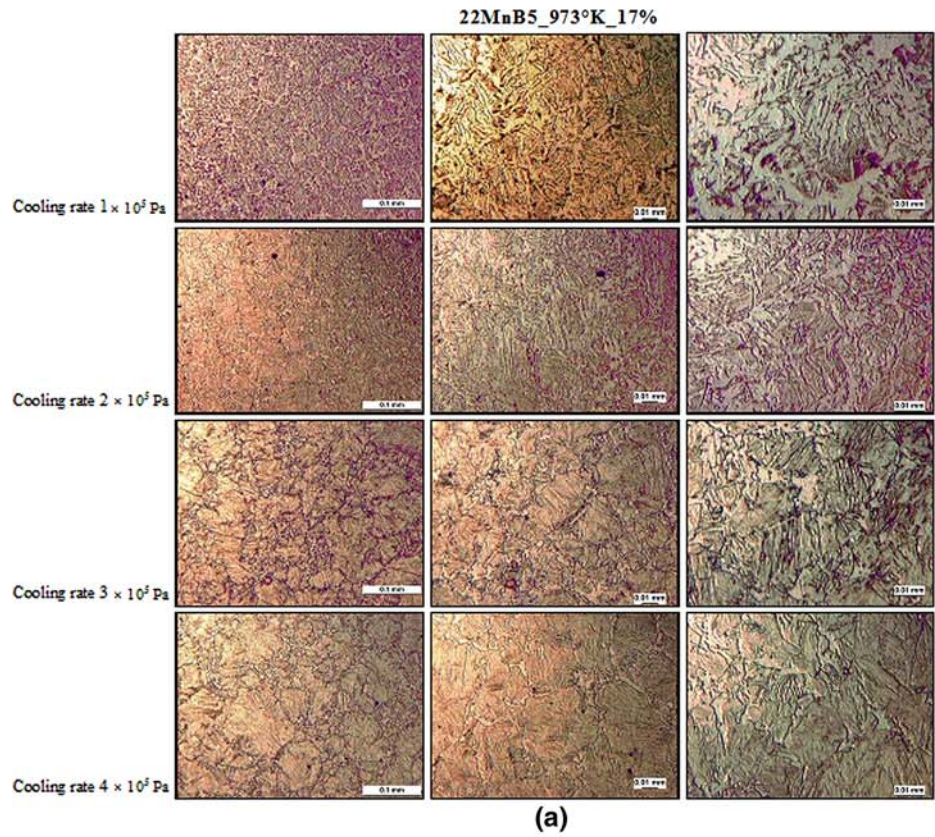


Fig. 10—(a) Micrographic analysis for four different cooling rates at 973 K and 17 pct of prestrain (magnifications 250 times–525 times–1250 times);  $1 \times 10^5$  Pa cooling rate 9 K/s,  $2 \times 10^5$  Pa cooling rate 22.5 K/s,  $3 \times 10^5$  Pa cooling rate 38.6 K/s, and  $4 \times 10^5$  Pa cooling rate 45.4 K/s. (b) Micrographic analysis for four different cooling rates at 973 K and 17 pct of prestrain (magnifications 250 times–525 times–1250 times);  $5 \times 10^5$  Pa cooling rate 50 K/s,  $6 \times 10^5$  Pa cooling rate 58.2 K/s,  $7 \times 10^5$  Pa cooling rate 66.1 K/s, and  $8 \times 10^5$  Pa cooling rate 77 K/s.

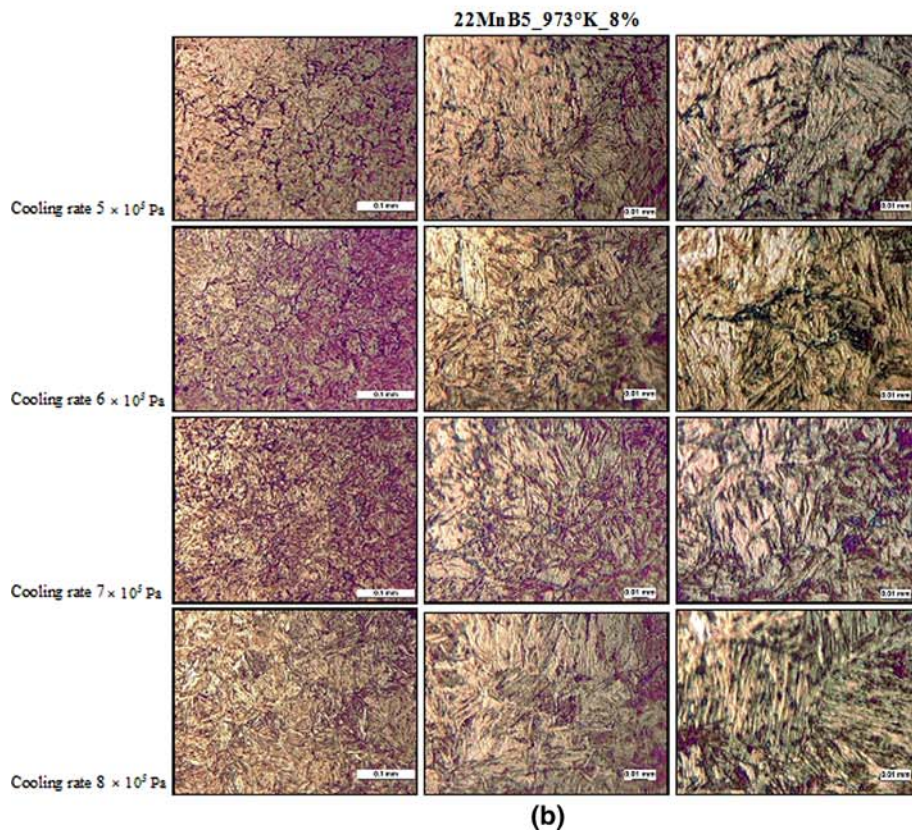
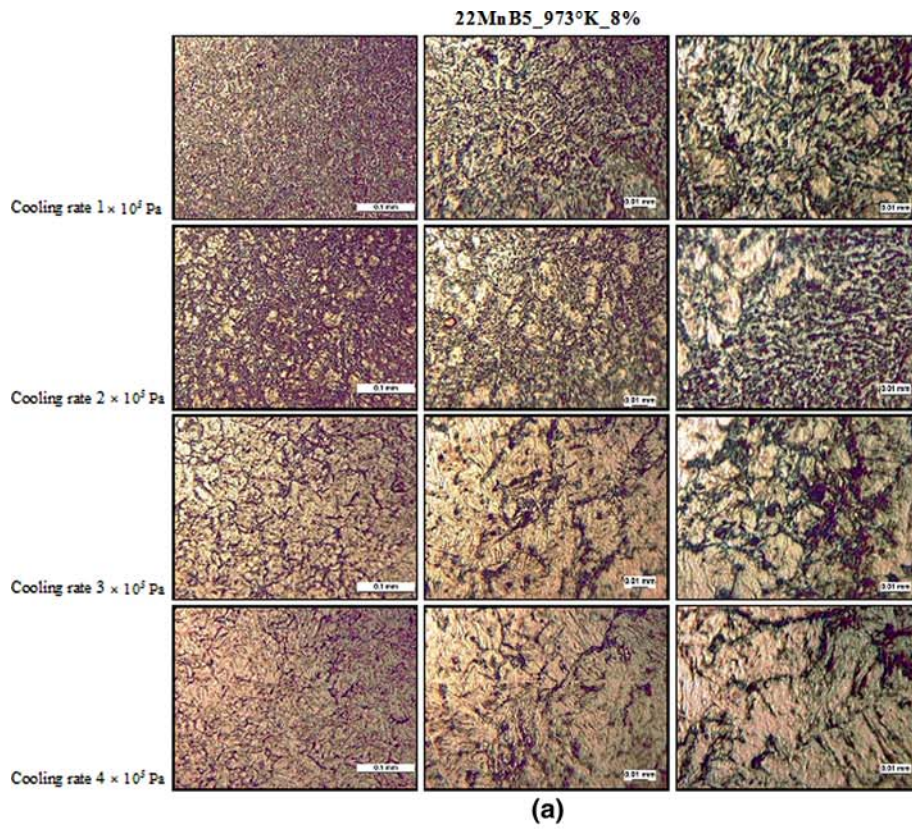


Fig. 11—(a) Micrographic analysis for four different cooling rates at 973 K and 8 pct of prestrain (magnifications 250 times–525 times–1250 times);  $1 \times 10^5$  Pa cooling rate 9 deg K/s,  $2 \times 10^5$  Pa cooling rate 22.5 K/s,  $3 \times 10^5$  Pa cooling rate 38.6 K/s, and  $4 \times 10^5$  Pa cooling rate 45.4 K/s. (b) Micrographic analysis for four different cooling rates at 973 K and 8 pct of prestrain (magnifications 250 times–525 times–1250 times);  $5 \times 10^5$  Pa cooling rate 50 K/s,  $6 \times 10^5$  Pa cooling rate 58.2 K/s,  $7 \times 10^5$  Pa cooling rate 66.1 K/s,  $8 \times 10^5$  Pa cooling rate 77 K/s.

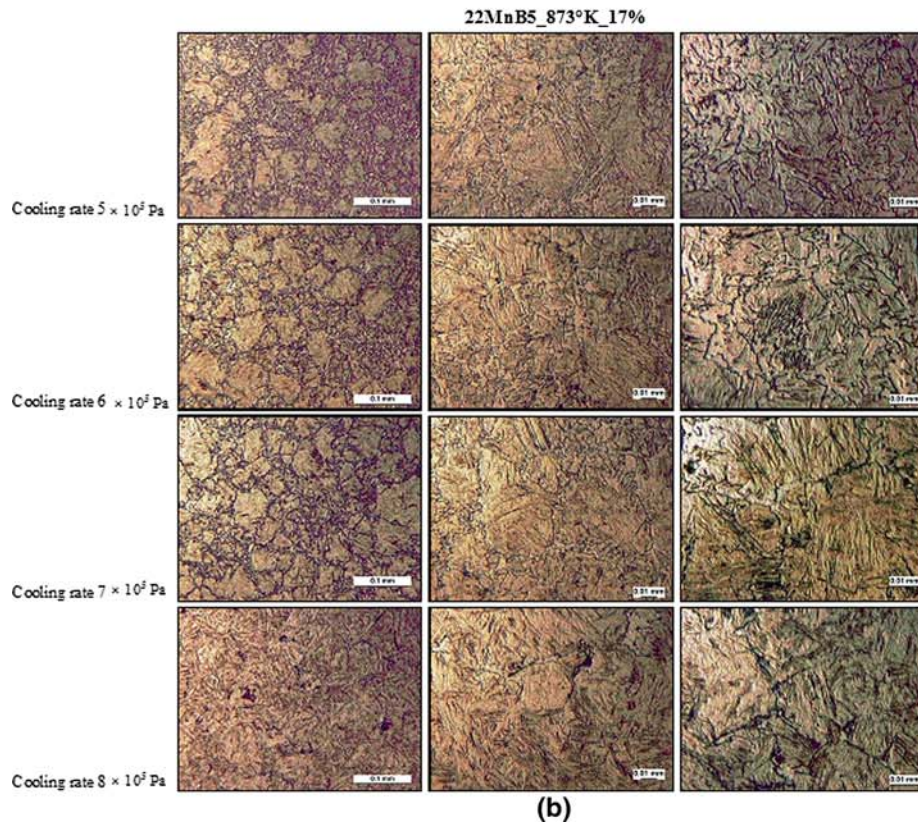
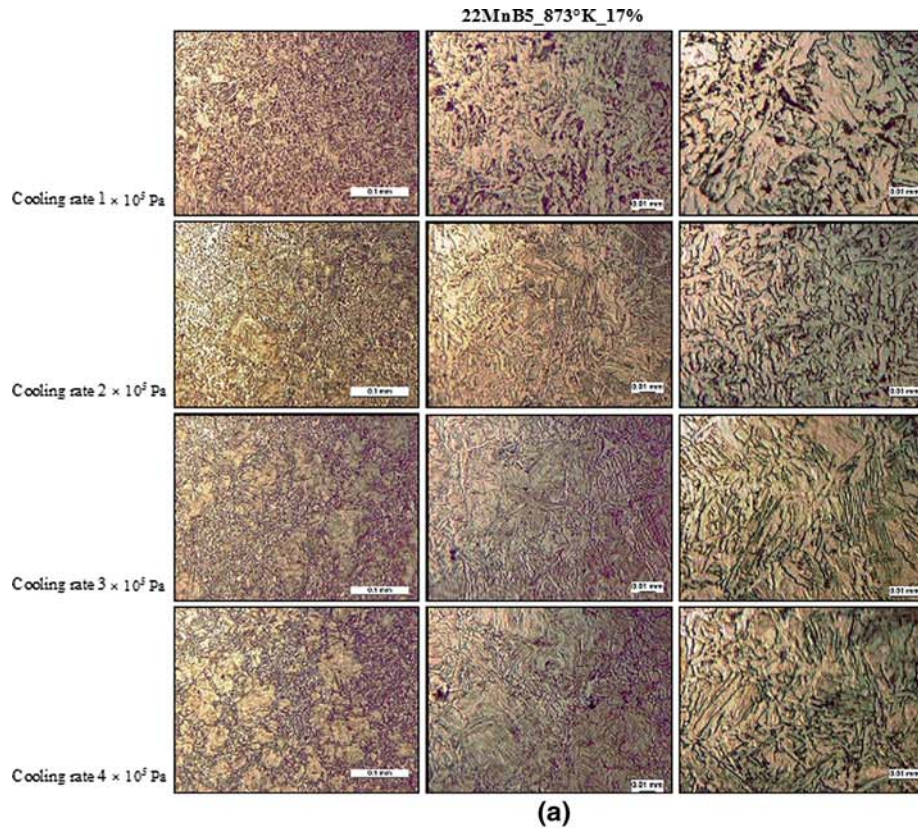


Fig. 12—(a) Micrographic analysis for four different cooling rates at 873 K and 17 pct of prestrain (magnifications 250 times–525 times–1250 times);  $1 \times 10^5$  Pa cooling rate 6.4 K/s,  $2 \times 10^5$  Pa cooling rate 15.1 K/s,  $3 \times 10^5$  Pa cooling rate 28.6 K/s, and  $4 \times 10^5$  Pa cooling rate 36.2 K/s. (b) Micrographic analysis for four different cooling rates at 873 K and 17 pct of prestrain (magnifications 250 times–525 times–1250 times);  $5 \times 10^5$  Pa cooling rate 40 K/s,  $6 \times 10^5$  Pa cooling rate 48.1 K/s,  $7 \times 10^5$  Pa cooling rate 54.1 K/s,  $8 \times 10^5$  Pa cooling rate 63.2 K/s.

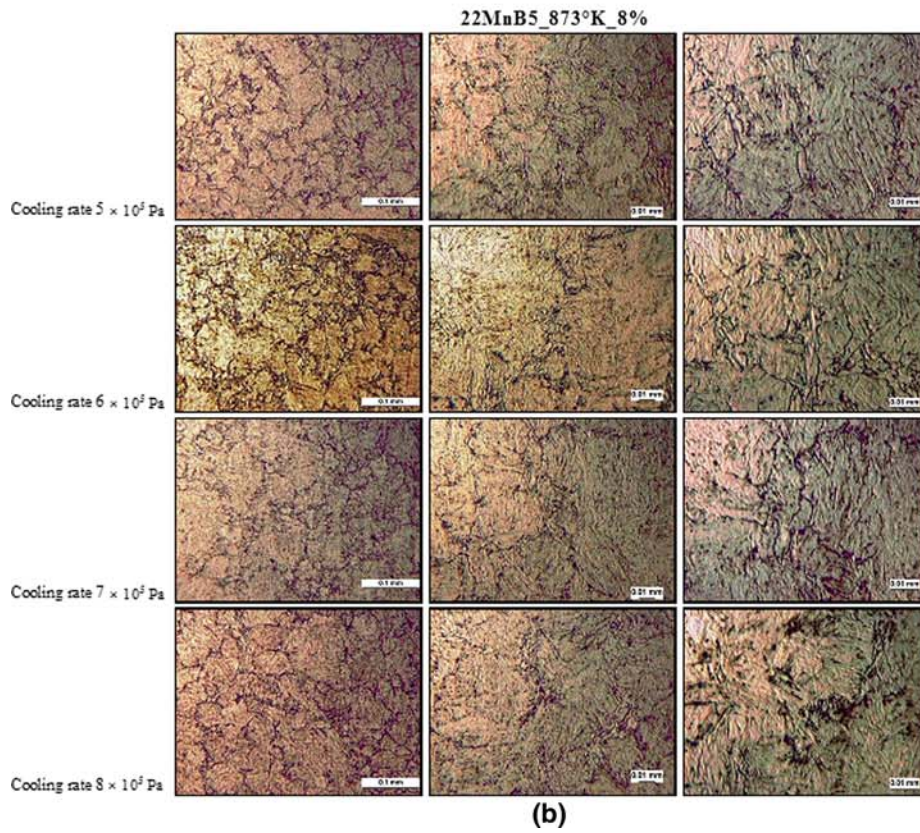
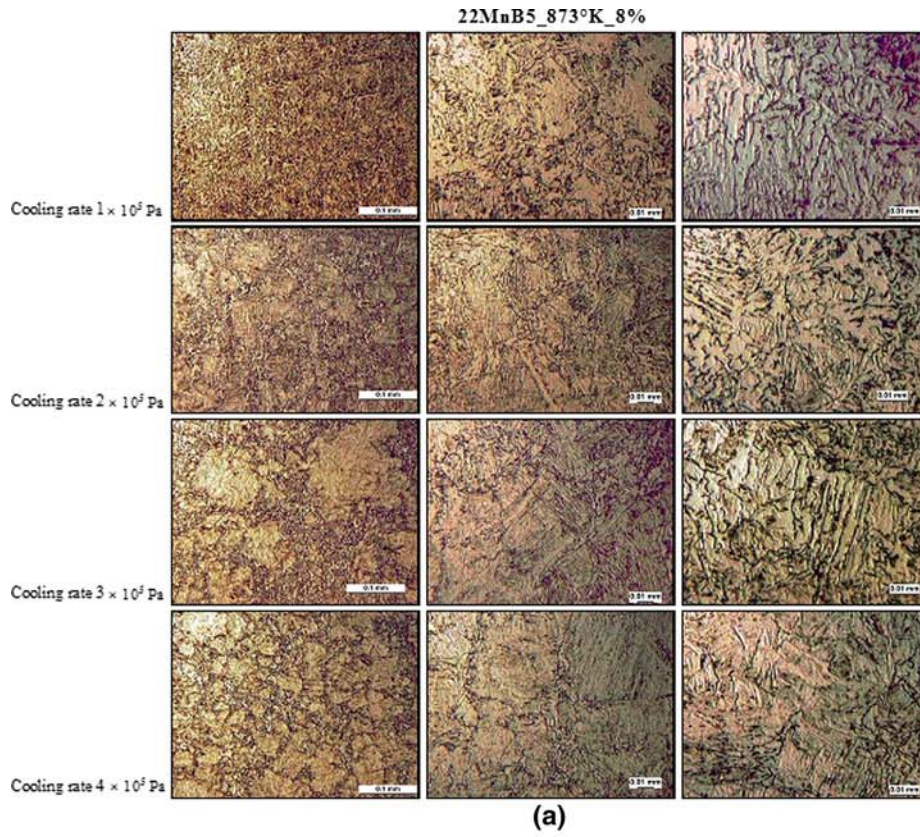


Fig. 13—(a) Micrographic analysis for four different cooling rates at 873 K and 8 pct of prestrain (magnifications 250 times–525 times–1250 times);  $1 \times 10^5$  Pa cooling rate 3.6 K/s,  $2 \times 10^5$  Pa cooling rate 8.1 K/s,  $3 \times 10^5$  Pa cooling rate 15.4 K/s,  $4 \times 10^5$  Pa cooling rate 26 K/s. (b) Micrographic analysis for four different cooling rates at 873 K and 8 pct of prestrain (magnifications 250 times–525 times–1250 times);  $5 \times 10^5$  Pa cooling rate 32.6 K/s,  $6 \times 10^5$  Pa cooling rate 38.9 K/s,  $7 \times 10^5$  Pa cooling rate 45.1 K/s,  $8 \times 10^5$  Pa cooling rate 51.2 K/s.

**Table II. Microhardness Vickers Values**

Prestrain	Cooling Rate							
	$1 \times 10^5$ Pa	$2 \times 10^5$ Pa	$3 \times 10^5$ Pa	$4 \times 10^5$ Pa	$5 \times 10^5$ Pa	$6 \times 10^5$ Pa	$7 \times 10^5$ Pa	$8 \times 10^5$ Pa
HV								
1223 K	290	482	533	551	551	551	551	551
1073 K 8 pct	251	482	515	533	533	533	551	551
1073 K 17 pct	269	482	515	515	533	533	551	551
973 K 8 pct	257	339	439	498	498	515	515	571
9730 K 17 pct	251	305	413	413	453	453	453	551
873 K 8 pct	251	321	401	426	498	498	498	515
873 K 17 pct	234	313	358	413	439	482	467	533

therefore necessary to preserve good mechanical strengths in the entire product. Figures 12(a) through 13(b) show the gradual microstructural modification through a constant lowering of the ferritic-pearlitic microstructure content at higher cooling rate. This observation suggests that the recrystallization phenomenon depends both on the hot deformation temperature and on the prestrain value. The micrographic results, in the case of the hot deformation temperature of 600 K, both for 8 and 17 pct of prestrain, manifest that the recrystallization process is more activated and produces a high amount of ferrite and pearlite phases also at high cooling rate (Figures 12(a) through 13(b)). The same influence of the prestrain value on the recrystallization phenomenon was found for the case of 973 K.

## VI. CONCLUSIONS

The method of press quenching of microalloyed boron steels allows response to the automotive industrial requirement in terms of safety and cost saving. The physical properties, and therefore the performances of hot-quenched components, are greatly influenced by the microstructure, residual stresses, and geometrical defects imposed by the manufacturing process.

In this work, the strains, transformation temperatures, microstructure, and microhardness properties of 22MnB5 steel, which was isothermally deformed under uniaxial tensile tests, were investigated at temperatures between 873 and 1223 K, using a fixed strain rate value of  $0.08 \text{ s}^{-1}$ . The experimental results evidenced that increasing hot deformation values generates lower HV values at the same cooling rate; this means that the increase of HPS shifts the CCT diagram toward lower times and, therefore, a lowering of the starting time for each transformation. Moreover, the obtained results evidenced that this phenomenon is inhomogeneous depending on the different temperature ranges of the diffusive transformations.

High values of hot deformations during the hot stamping process, therefore, require a strict control of the cooling process in order to ensure cooling rate values that allow maintaining good mechanical characteristics of components. The recrystallization phenomenon depends on the HPS temperature, the residence time at elevated temperature, and finally on the hot deformation

level. The occurrence of the PAGS refinement, produced from the recrystallization process, influences the kinetics of the austenitic diffusive transformations and, therefore, influences the amount of ferrite and pearlite that can be formed during the hot deformation process. Finally, the HPS generates a reduction in  $M_s$  and  $M_f$  temperatures, but this reduction becomes smaller when the temperature of HPS decreases. The feasible future outlook is the development, starting from this wide microstructural base knowledge, of a neuro-fuzzy model able to predict the microstructure and the mechanical properties of the material under different hot deformation conditions.<sup>[22,23]</sup>

## ACKNOWLEDGMENT

The authors thank the Lehrstuhl für Fertigungstechnologie of the University of Erlangen-Nuremberg that provided the experimental setup and the material for this study.

## REFERENCES

1. P. Åkerström, B. Wikman, and M. Oldenburg: *Mater. Sci. Eng.*, 2005, vol. 13, pp. 1291–1308.
2. M. Eriksson, M. Oldenburg, M.C. Somani, and L.P. Karjalainen: *Mater. Sci. Eng.*, 2002, vol. 10, pp. 277–94.
3. M.-C. Zhao, K. Yang, F.-R. Xiao, and Y.-Y. Shan: *Mater. Sci. Eng.*, 2003, vol. A355, pp. 126–36.
4. K.A. Taylor and S.S. Hansen: *Metall. Trans. A*, 1990, vol. 21A, p. 1697.
5. K.A. Taylor: *Metall. Trans. A*, 1992, vol. 23A, p. 107.
6. S.K. Banerji and J.E. Morral: *Boron in Steel*, TMS-AIME, Warrendale, PA, 1980.
7. E. Lopez-Chipres a, I. Mejia, C. Maldonado, A. Bedolla-Jacuinde a, M. El-Wahabi, and J.M. Cabrera: *Mater. Sci. Eng. A*, 2007, vols. 460–461, pp. 464–70.
8. Z.-G. Yang and H.-S. Fang: *Curr. Opin. Solid State Mater. Sci.*, 2005, vol. 9, pp. 277–86.
9. P. Åkerström and M. Oldenburg: *J. Mater. Process. Technol.*, 2006, vol. 174, pp. 399–406.
10. M. Naderi, L. Durrenberger, A. Molinari, and W. Bleck: *Mater. Sci. Eng. A*, 2008, vol. 478 (1–2), pp. 130–39, ISSN: 09215093.
11. M. Geiger, M. Merklein, and C. Hoff: *Proc. SCT2005*, Verlag Stahleisen GmbH, Wiesbaden, Germany, 2005, pp. 179–86.
12. M. Merklein, J. Lechler, and M. Geiger: *Ann. CIRP*, Kobe, Japan, 2006, vol. 55.
13. H.K.D.H. Bhadeshia: *Bainite in Steels*, Institute of Materials, London, 2001.

14. K. Hase, C. Garcia-Mateo, and H.K.D.H. Bhadeshia: *Mater. Sci. Technol.*, 2004, vol. 20, pp. 1499–1505.
15. H.J. Jun, J.S. Kanga, D.H. Seo, K.B. Kang, and C.G. Park: *Mater. Sci. Eng. A*, 2006, vol. 422, pp. 157–62.
16. H.-L. Yi, L.-X. Du, G.-D. Wang, and X.-H. Liu: *J. Iron Steel Res. Int.*, 2006, vol. 13 (3), pp. 36–39 and 67.
17. S. Morito, H. Saito, T. Ogawa, T. Furuhashi, and T. Maki: *ISIJ Int.*, 2005, vol. 45 (1), pp. 91–94.
18. A. Ardehali Barani, F. Li, P. Romano, D. Ponge, and D. Raabe: *Mater. Sci. Eng. A*, 2007, vol. 463, pp. 138–46.
19. N. Nakata and M. Militzer: *ISIJ Int.*, 2005, vol. 45 (1), pp. 82–90.
20. W. Garlipp, M. Cilense, and S.I. Novaes Gomes: *J. Mater. Proc. Technol.*, 2001, vol. 114, pp. 71–74.
21. A. Barcellona and D. Palmeri: *Proc. 8th Int. Conf. on Advanced Manufacturing Systems and Technology AMST '08*, SpringerWien NewYork, Udine, Italy, 2008, pp. 571–82.
22. R. Kaspar, W. Kapellner, and O. Pawelski: *Steel Res.*, 1986, vol. 57 (11), pp. 557–62.
23. C.H. Lee, H.K.D.H. Bhadeshia, and H.-C. Lee: *Mater. Sci. Eng. A*, 2003, vol. 360, pp. 249–57.